Diagnosis of Spatial Distribution and Low Energy Level Density of Argon Plasma Jet Active Particles

Dawei Zhang(✉), Xiaoying Chen, and Sha Hao

Shenyang Ligong University, Shenyang 110159, Liaoning, China
springdavid@163.com

Abstract. With the deepening of the application of atmospheric pressure low-temperature plasma in the field of biomedicine, the accurate regulation of active particle components and doses also needs to be broken, and all aspects of plasma still need to be studied in depth. Based on this, Ben In this paper, a needle-ring electrode was used to build a plasma discharge device to study the characteristics of 0.1 MPa argon plasma jet number, plasma irradiation at 4 mm, 8 mm, 12 mm, 16 mm, 20 mm away from the nozzle was collected degree, analyze the change law of the type and number of active particles in argon plasma. The results showed that argon plasma. The active particles are mainly oxygen atoms and hydroxyl groups; When argon plasma acts on the copper foil, the surface of the copper foil is low in argon. The relationship between the density of energy levels is $ns_4 > ns_5 > ns_2 > ns_3$; Metastable ($1s_3$ and $1s_5$) number density versus resonant state ($1s_2$ Similar to $1s_4$), the number density changes the linear type, and the change trend increases first and then decreases with the increase of axial distance. This paper provides methods and ideas for the generation and optimization of argon plasma jet and the optimization of diagnostic methods, and establishes plasmacy. The control model of the descendant provides a reference and basis.

Keywords: active particles · metastability · resonance state · Number density

1 Introduction

Atmospheric pressure cold plasma has a wide range of applications in the biomedical field, among which the most concerned include: biomutagenesis breeding, disinfection and sterilization, wound treatment, cosmetic and dermatological treatment, tooth whitening and root canal disinfection, cancer treatment, etc. [1]. Plasma jets greatly broaden the scope of application of plasma medicine because they can generate plasma in an open space, so that the treated sample is not limited by the size of the discharge gap [4].

With the rapid development of plasma biomedicine in the past 20 years, some new key problems need to be broken, and the accurate regulation of active particle components and dosage [2] is one of them. A large number of studies have found that the biomedical effects of plasma are mainly achieved through active particles, including charged particles, oxygen-containing active particles, nitrogenous active particles, etc. Therefore,

D. Dai et al. (Eds.): ISPEC 2022, SPPHY 391, pp. 245–255, 2023.
https://doi.org/10.1007/978-981-99-1576-7_24

in plasma biomedical applications, it is ultimately necessary to control the composition and dose of these active particles [2], and Lu Xinpei et al. of Huazhong University of Science and Technology proposed the equivalent total oxidation potential as the plasma dose for the leading role of reactive oxygen species in plasma biological effects, which is a major breakthrough for the application of plasma in medicine. Yue Yuanfu [5], a student of Lu Xinpei, applied laser-induced fluorescence spectroscopy to diagnose and optimize hydroxyl and oxygen atoms in atmospheric pressure low-temperature plasma jets. Senior brother Yang Chen [3, 6] used PLS-800 equipment and argon plasma jet spray gun to confirm the composition in the argon plasma jet. At present, the regulation of active particle components and dosage still faces the problem that the microscopic mechanism of plasma chemistry is not clear enough, and it is difficult to comprehensively consider various factors to achieve fine control. In view of this, it is necessary to take a variety of measures to break down complex plasma chemistry [7], classify and study the biomedical effects of active particles at a quantitative level; It is necessary to precisely control the plasma generation conditions, especially to fully consider the influence of surrounding environmental factors, so that the active particle components and doses generated during the discharge process remain unchanged under different environmental conditions and in the long-term operation of the plasma source.

Based on this, this paper builds a plasma generation device under the needle-ring electrode structure, generates argon plasma jet in an open environment of 0.1 MPa, uses emission spectroscopy to obtain spectral data of different axial distances in the plasma jet process, analyzes the changes of active particles in argon plasma, calculates the number density of argon metastable state and resonance state, and analyzes and discusses its change law.

2 Argon Plasma Jet Experimental Platform Established

The experimental platform can be divided into three parts, namely the drive power supply [8], needle-ring discharge electrode, and spectral acquisition diagnostic system. Among them, the drive power supply is composed of 0–220 V adjustable DC power supply, PWM drive unit, half-bridge circuit and resonant high-voltage transformer. The output frequency is adjustable from 15–40 kHz, and the voltage amplitude is adjustable from 0–15 kV; The high-voltage electrode of the needle-ring discharge electrode is a copper rod with a length of 30 mm and a diameter of 1mm, the ground electrode is a copper ring with a width of 6 mm, and the length of the high-voltage electrode from the ground electrode is 6 mm. The insulating medium is a uniform texture quartz glass tube with a length of 50 mm, an inner diameter of 6 mm and an outer diameter of 8 mm. The plasma generation and measurement device is shown in Fig. 1, wherein the working gas is argon with a volume fraction of 99.99%, and the spectrometer model used for the experimental acquisition of plasma emission spectroscopy is ULS2048-USB2. In order to exclude the influence of external light sources on the experimental results, this experiment was carried out with the lights turned off at night.

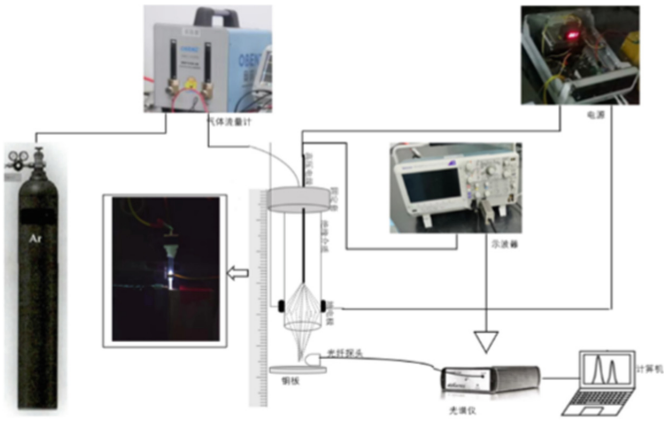

Fig. 1. Plasma generation and measurement device

2.1 Pin-to-Ring Discharge Electrode

Compared with other dielectric blocking discharge electrode structures, the biggest difference is that the ground electrode is above the high-voltage electrode, so that the electrons generated by the discharge at the tip of the needle are more likely to migrate to the ground electrode driven by the air flow, thus forming a plasma jet. In addition, the electric field strength at the tip of the needle is large, and it is easy to discharge to generate plasma. As a result, the plasma jet source can break down the gas at lower voltages, creating a discharge-stable plasma jet.

2.2 Plasma Spectral Acquisition System

In the experiment, the working gas is first introduced into the discharge device, the power supply is turned on, the voltage value is adjusted, the plasma is observed to observe whether the discharge nozzle is generated, and the spectrum is acquired when the nozzle produces a relatively stable plasma jet. Treat the glass tube spout as the starting point as 0 cm. It is observed that the length of the plasma natural jet produced by this experimental device under different input voltages is different, and the maximum jet length is 20 mm. Taking the distance from copper foil to glass tube nozzle as the independent variable, considering the experimental operability, 4 mm intervals were selected, that is, the distances between copper foil and glass tube nozzle were 4 mm, 8 mm, 12 mm, 16 mm, and 20 mm, respectively, and plasma spectral data were collected.

During the experiment, it is always ensured that the fiber optic probe and the glass tube mouth of the needle-loop discharge device are on the same horizontal line, and the distance between the optical fiber probe and the copper foil is always consistent at 2 mm. The experiment was repeated at least ten times, and three sets of spectral data were saved under the same experimental conditions at each distance to ensure the accuracy of the experimental results and reduce the influence of accidental factors on the experimental results.

2.3 Plasma Spectroscopy Analysis System

When the plasma system is affected by external factors such as electric field, the particle number density of the excited state increases. But excited particles are inherently extremely unstable and short-lived, and they transition to lower energy levels and release photons through spontaneous and stimulated radiation, a process that forms the emission spectrum. Different kinds of particles correspond to different wavelengths of emission spectral lines, so the emission spectrum can diagnose the specific particle species in the plasma discharge system.

In addition, the parameters of other plasmas can also be obtained by the analysis of emission spectroscopy, and the emission spectroscopy method is used to acquire the spectra in the plasma jet process. Through Avasoft software, the irradiance changes of each particle spectral line in the plasma can be intuitively observed, and the generated Excel table contains the accurate value of the irradiance of each particle wavelength of the plasma, and important parameters such as electron temperature and electron density can be obtained through the analysis of irradiance.

3 Spatial Distribution of Argon Plasma Jets

In the experiment, the spectrum is acquired by spectrometer (effective range of 200–1000 nm), where the abscissa is the wavelength, and the particle type can be determined; The ordinate is irradiance, which refers to the radiation flux that falls on the surface area of the unit detector.

3.1 Particle Species and Spatial Distribution

After analysis, it is found that the length of argon plasma jet produced by the needle-ring discharge device starting from the nozzle is 20 mm, and a total of 22 argon atomic lines at 690–1000 nm, 21 nitrogen molecular lines at 300–500 nm, 1 hydroxyl radical line at

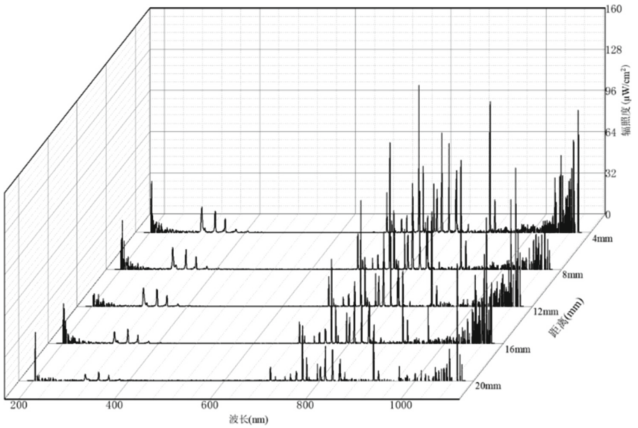

Fig. 2. Spectral line variation plot of each particle increasing with distance

306–318 nm, and 2 oxygen atom lines at 750–850 nm were collected. The spectral lines of each particle increase with axial distance are shown in Fig. 2.

With the increase of the distance between the copper plate and the nozzle, the irradiance of each particle gradually decreases. The highest irradiance at 4 mm, which may be due to the fact that at 4 mm, the plasma acts on the copper plate closestly, and the copper plate has an adsorption effect on the plasma, so that more particles move along the glass tube nozzle to the copper plate, accumulating near the copper plate to increase the irradiance.

This device adopts sinusoidal AC power supply, and the gas flow rate is adjusted by the gas flow meter, and the length of the jet is related to the gas flow rate. According to the theory of gas dynamics, it is divided into laminar flow, transition state and turbulent flow by Reynolds number [8]. Re = ρνd/μ where: the working gas is argon, ρ take 1.6228 kg/m^3; ν is the gas flow rate, m/s; d is the diameter of the glass tube, d = 6 × 10^{-3} m, μ is the kinematic viscosity coefficient, take 2.23 × 10 − 5 kg/(m · s) [9]. When Re < 2300, the gas flow is in a laminar flow state; When 2300 < Re < 8000, the gas flow is in a transitional state; When Re > 8000, the gas flow is in turbulent state [10]. According to the formula: when Re = 2300, v = 5.27 m/s; When Re = 8000, v = 18.32 m/s. According to a large number of studies in fluid dynamics, the length of the jet produced when the gas flow is in a transitional state is the maximum [11], that is, the maximum length of the jet should theoretically occur between 5.27 m/s and 18.32 m/s in argon flow velocity. The gas flow rate in this experiment is about 12 m/s, which belongs to the transition state, and the maximum length of the plasma jet is 20 mm, and the place with the largest number of plasma particles is 4 mm.

3.2 Spatial Distribution Analysis of Active Particles

The active particles in the argon plasma jet are oxygen atoms and OH radicals, and the irradiance changes of the three active particles are shown in Table 1 below.

Table 1. Irradiance of active particles at different distances

Active particles	wavelength λ(nm)	4 mm I(μW/cm^2)	8 mm I(μW/cm^2)	12 mm I(μW/cm^2)	16 mm I(μW/cm^2)	20 mm I(μW/cm^2)
Oxygen atoms	777.5	1.16	1.39	1.63	0.89	0.76
Oxygen atoms	844.6	1.01	1.18	1.32	1.04	0.95
OH	308	9.48	7.77	7.08	3.35	2.77

It can be seen from the table that the irradiance of oxygen atoms increases first and then decreases with the increase of the distance from the copper foil to the surface of the material, and the irradiance of OH radicals gradually decreases with the increase of the distance from the copper foil to the surface of the material and the analysis of the gradual decrease in the irradiance of oxygen atoms suggests that the oxygen atoms in the

atmospheric pressure low-temperature plasmonic jet are mainly the following reactions [14]:

$$\begin{gathered} e + O_2 \rightarrow O^* + O + e \\ O^* + Ar \rightarrow O + Ar \\ e + O_2 \rightarrow O + O^* + e \\ e + O_2 \rightarrow 2O + e \end{gathered}$$

Oxygen atoms are mainly produced by the reaction of electrons and metastable oxygen atoms with gas molecules or atoms. During the experiment, the plasma jet came into contact with the air, and it is obviously unrealistic to assume that oxygen atoms do not react with other particles since they are generated. The reaction of oxygen atoms and other particles is bound to cause the attenuation of oxygen atoms, coupled with the impact of the life of oxygen atoms themselves, which will inevitably cause the irradiance to show a downward trend or even disappear.

According to the analysis of the gradual decrease of OH irradiance, the mechanism of free radicals in atmospheric pressure low-temperature plasmonic jets [12] mainly comes from electron collision, metastable particle decomposition, ion-electron and ion-ion recombination, etc. [13]. These processes are mainly concentrated during or in a very short time after discharge, and the subsequent processes are mainly the disappearance and attenuation of free radicals [15]. In argon plasma, the first excited state OH(A2Σ+) is produced by the collision of high-energy electrons e* in the plasma and argon atom Ar* in the excited state with water vapor doped in the air, respectively [15, 16].

$$\begin{gathered} e^* + H_2O \rightarrow OH\left(A^2\Sigma+\right) + H + e \\ Ar^* + H_2O \rightarrow OH\left(A^2\Sigma+\right) + Ar + H \\ OH(A2\Sigma+) \rightarrow OH\left(X^2\Pi\right) + hv \end{gathered}$$

The disappearance and attenuation of free radicals is mainly affected by chemical reactions, free diffusion, surface adsorption, and gas flow [15]. In the atmospheric pressure low-temperature plasma jet, because the jet is in direct contact with the air, OH radicals may also react with some other particles such as O, O2, etc., and some of the reaction formulas are as follows [11],

$$\begin{gathered} OH + O \rightarrow O_2 + H \\ OH + H \rightarrow H_2O \\ OH + O_2 \rightarrow HO_2 + O \end{gathered}$$

These reactions are another important attenuation mechanism for free radicals in atmospheric pressure low-temperature plasma jets. In addition, OH free radicals themselves have a certain lifespan, assuming that OH does not react with other particles since it is generated, as long as the collection time during the experiment exceeds the life of the OH free radical itself, then OH free radicals will disappear. Therefore, these factors may cause OH irradiance to decrease or even disappear.

Therefore, in this experiment, when the distance between the copper plate and the glass tube nozzle increases, the irradiance of OH radicals decreases, partly due to the life

of OH radicals themselves, and partly due to the chemical reaction between OH radicals and other particles in the air.

According to the irradiance change of each particle, in order to further study the argon plasma discharge mechanism, the argon metastable state and resonance state density in the argon plasma jet process are calculated and analyzed.

4 Argon Metastable and Resonant State Density Calculation

In plasma, an optical transition from energy level i to energy level j occurs at the r position, and photons with a frequency of v_0 (or wavelength λ_0) are emitted during this optical transition. In general, only a portion of photons can leave the plasma volume, while other photons are reabsorbed by J-class atoms as they are transported through the plasma. In spatially resolved OES measurements, only photons emitted along the line of sight are considered, in which case a one-way escape factor (r_{ij}) can be used to describe the self-absorption effect [13]. Assuming that the atomic density of class i is n_i and the Einstein coefficient of i to j is A_{ij}, the emission intensity can be expressed as [19]

$$I_{ij}(r) = r_{ij}A_{ij}n_i \tag{1}$$

We consider a transition from a common high energy level i to different lower levels j and k, and the emission intensity ratio can be expressed as:

$$\frac{I_{ij}(r)}{I_{ik}(r)} = \frac{r_{ij}A_{ij}}{r_{ik}A_{ik}} \tag{2}$$

As can be seen from the above equation, the spectral line emission intensity ratio depends on the escape factor and Einstein coefficient, and is independent of the n_i of the upper energy level density. By using a global approximation of the escape factor, the analysis can be greatly simplified. In the work of this article, we use Mewe's expression [20]:

$$r_{ij} \approx \frac{2 - \exp\left(-10^{-3}k_{ij}(\Delta v = 0)L\right)}{1 + k_{ij}(\Delta v = 0)L} \tag{3}$$

where L is the plasma volume depth accessible to the photon detector, and k_{ij} ($\Delta v = 0$) is the absorption coefficient [19], defined as:

$$k_{ij}(\Delta v) = \frac{\lambda_{ij}^2}{8\pi}P_{ij}(\Delta v)\frac{g_i}{g_j}\overline{n}_j A_{ij} \tag{4}$$

where λ_{ij} is the wavelength, g_i and g_j are statistical weights, n_j is the low-level density, and P_{ij} is the spectral line frequency distribution.

This experiment is carried out in an atmospheric pressure environment, the spectral line is affected by these four mechanisms, combined with the literature that has been consulted, this paper only calculates the logarithmic density from the Doppler broadening angle to analyze the change trend of the number density. When the Doppler effect is the

main broadening mechanism, the spectral line frequency distribution P_{ij} [21] is defined as:

$$P_{ij} = \lambda_{ij}\sqrt{\frac{m}{2\pi k_B T}} \tag{5}$$

where m is the mass of the atom, k_B is the Boltzmann constant, and T is the gas temperature.

In summary, the emission intensity ratio can be expressed as [22] for the transition from a common high energy level i to different lower energy levels j and k

$$\frac{I_{pi-sj}}{I_{pi-sk}} = \frac{\frac{2-\exp\left(-10^{-3}C_{pi-sj}n_{sj}l/\sqrt{T_g}\right)}{1+C_{pi-sj}n_{sj}l/\sqrt{T_g}}}{\frac{2-\exp\left(-10^{-3}C_{pi-sk}n_{sk}l/\sqrt{T_g}\right)}{1+C_{pi-sk}n_{sk}l/\sqrt{T_g}}}\frac{A_{pi-sj}}{A_{pi-sk}} \tag{6}$$

where C_{pi-sj} is

$$C_{pi-sj} = \frac{\lambda_{pi-sj}^3}{8\pi}\frac{g_{pi}}{g_{sj}}\sqrt{\frac{m}{2\pi k_B T}}A_{pi-sj} \tag{7}$$

The spectral lines and associated parameters selected for calculating metastable ($1s_3$ and $1s_5$ levels) and resonant density ($1s_2$ and $1s_4$ levels) are shown in Table 2.

Most of these lines have strong emission intensity in the visible range. The experiment selected the ratio of the cooperation intensity of two sets of spectral lines with the same upper energy level. The specific combination arrangement is as follows: $2p_2 \rightarrow 1s_5$, $2p_2 \rightarrow 1s_2$; $2p_2 \rightarrow 1s_4$, $2p_2 \rightarrow 1s_2$; $2p_3 \rightarrow 1s_5$, $2p_3 \rightarrow 1s_2$; $2p_3 \rightarrow 1s_4$, $2p_3 \rightarrow 1s_2$; $2p_4 \rightarrow 1s_3$, $2p_4 \rightarrow 1s_2$. A total of five combinations were selected to establish a system of equations, and the density of metastable states ($1s_3$ and $1s_5$ energy levels) and resonant state densities ($1s_2$ and $1s_4$ energy levels) was fitted by the least squares method. Make

Table 2. Argon emission lines used to calculate metastable and resonant state densities [23]

number	$\lambda(nm)$	$A_{ki} \times 10^6$ (s^{-1})	Paschen	g_i	g_j
1	826.45	1.53	$2_{P2} \rightarrow 1_{S2}$	3	3
2	727.29	1.83	$2_{P2} \rightarrow 1_{S4}$	3	3
3	696.54	6.39	$2_{P2} \rightarrow 1_{S5}$	3	5
4	840.82	22.3	$2_{P3} \rightarrow 1_{S2}$	5	3
5	738.4	8.47	$2_{P3} \rightarrow 1_{S4}$	5	3
6	706.72	3.8	$2_{P3} \rightarrow 1_{S5}$	5	5
7	852.14	13.9	$2_{P4} \rightarrow 1_{S2}$	3	3
8	794.84	18.6	$2_{P4} \rightarrow 1_{S3}$	3	1

D minimal during fitting [24]:

$$D = \sum_i \sum_j \sum_k \left(\frac{I_{i\to \mathrm{j}}}{I_{i\to \mathrm{k}}} - \frac{r_{ij}A_{ij}}{r_{ik}A_{ik}} \right)^2 \tag{8}$$

The trend of number density changes in metastable states ($1s_3$ and $1s_5$ energy levels) and resonant state densities ($1s_2$ and $1s_4$ energy levels) at different distances is plotted as shown in Fig. 3.

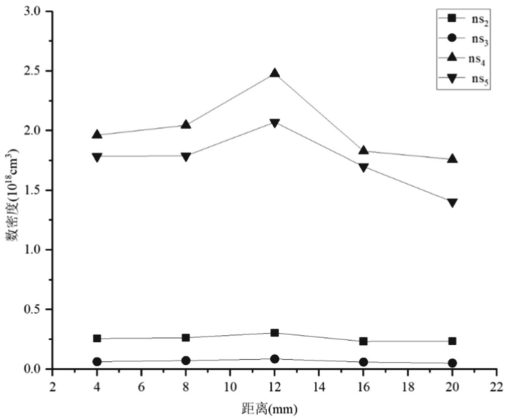

Fig. 3. Trend chart of number density change

It can be seen from Fig. 3 that with the increase of the distance between the copper plate and the glass nozzle, the metastable and resonance state number density of argon shows a trend of first increasing and then decreasing, which is different from the trend of particle irradiance gradually decreasing with the increase of distance. When the distance from the copper plate to the glass nozzle is 4 mm, 8 mm, 12 mm, 16 mm, and 20 mm, the number density relationship is $ns_4 > ns_5 > ns_2 > ns_3$, and when the distance is 4 mm, 8 mm, 12 mm, 16 mm, 20 mm, the number density of the $1s_5$ energy level is similar to the density of the $1s_4$ energy level, and the number density of the $1s_2$ energy level is similar to the number density of the $1s_3$ energy level.

It is believed that the ionization energy of argon metastable atoms and the excitation energy to higher excited states are smaller than those of ground state atoms, and the vast majority of low-energy electrons in the plasma can directly ionize or excite argon metastable atoms to higher energy levels, making them the most important source of electrons, ions and highly excited particles in addition to ground state argon atoms [25]. For the obtained number density relationship $ns_4 > ns_5 > ns_2 > ns_3$, the analysis believes that argon plasma is produced in atmospheric pressure air in the experiment, and when the plasma acts on the copper foil, the particle irradiance increases, the particle reacts more violently, and a large number of low-energy electrons will excite the metastable argon atom to a higher energy level. In addition, due to the energy it carries, argon metastable atoms can decompose gas molecules to produce active particles in the mixed discharge

of argon gas and other molecular gases [26], so the resulting metastable number density will be lower than that of the resonance state.

5 Conclusion

In this paper, a needle-ring medium is used to block the plasma discharge device to generate a stable argon plasma jet under atmospheric pressure conditions, and its spectral data are collected and diagnosed, and the metastable and resonant state number density changes of the active particles and argon acting on the surface of copper foil by argon plasma jet are studied, and the results show that:

The active particles in the argon plasma jet produced by the needle-ring type medium that blocks the plasma discharge device in atmospheric pressure air are mainly oxygen atoms and hydroxyl radicals; When argon plasma acts on the copper plate, the oxygen atom increases first and then decreases with the increase of the distance from the copper plate to the nozzle, and the hydroxyl radical gradually decreases.

When argon plasma is applied to the copper plate, the relationship between the metastable ($1s_3$ and $1s_5$) number density of argon and the number density of the resonant state ($1s_2$ and $1s_4$) is $ns_4 > ns_5 > ns_2 > ns_3$, and the number density of metastable ($1s_3$ and $1s_5$) is similar to that of the resonant state ($1s_2$ and $1s_4$), and the trend of first increasing and then decreasing with the increase of axial distance.

References

1. Zhang, X., Zhang, X.F., Li, H.P., et al.: Atmospheric and room temperature plasma (ARTP) as a new powerful mutagenesis tool (mini review). Appl. Microbiol. Biotechnol. **98**(12), 5387–5396 (2014)
2. Kong, M.G., Kroesen, G., Morfill, G., et al.: Plasma medicine: an introductory review. New J. Phys. **11**(11), 115012 (2009)
3. Lloyd, G., Friedman, G., Jafri, S., et al.: Gas plasma: medical uses and developments in wound care. Plasma Process. Polym. **7**(3–4), 194–211 (2010)
4. Lu, X.: High Voltage Eng. **37**(06), 1416–1425 (2011)
5. Yue, Y.: Diagnosis and optimization of hydroxyl and oxygen atoms in atmospheric pressure plasma jet. Huazhong University of Science and Technology (2017)
6. Yang, C.: Spatial distribution analysis of argon plasma jet spectroscopy. China Equip. Eng. **2022**(03), 16–18 (2022)
7. Wang, F.: Computational Fluid Dynamics Analysis - Principles and Applications of CFD Software. Tsinghua University Press, Beijing (2004)
8. Li, Z.: Research on cold plasma jet technology for wound suture. Shenyang University of Science and Technology (2016)
9. Miles, R.B., Lempert, W.R., Forkey, J.N.: Laser Rayleigh scattering. Meas. Sci. Technol. **12**(5), R33 (2001)
10. Dilecce, G., Ambrico, P.F., Simek, M., De Benedictis, S.: LIF diagnostics of hydroxyl radical in atmospheric pressure He-H2O dielectric barrier discharges. Chem. Phys. **398**, 142–147 (2012)
11. Irons, F.E.: J. Quant. Spectrosc. Radiat. Transfer **22**, 1 (1979)
12. Li, J., et al.: J. Phys. D: Appl. Phys. **44**, 292001 (2011)
13. Breton, C., Schwob, J.L.: C. R. Acad. Sci. Paris **260**, 461 (1965)

14. Pei, X.: Research on atmospheric pressure low-temperature plasma jet source and diagnosis of its key active particles. Huazhong University of Science and Technology (2014)
15. Schulze, M., Yanguas-Gil, A., von Keudell, A., Awakowicz, P.: A robust method to measure metastable and resonant state densities from emission spectra in argon and argon-diluted low pressure plasmas. J. Phys. D: Appl. Phys. **41**(6), 065206 (2008)
16. Mewe, R.: Z. Naturf. a **25**, 1798 (1970)
17. Lymberopoulos, D.P., Economou, D.J.: Fluid simulations of glow discharges: effect of metastable atoms in argon. J. Appl. Phys. **73**, 3668–3679 (1993)
18. Ali, A.W., Griem, H.R.: Theory of resonance broadening of spectral lines by atom-atom impacts. Phys. Rev. **140**(4A), A1044 (1965)
19. Measurement of Ar resonance and metastable level number densities in argon containing plasmas. J. Phys. D: Appl. Phys. **43**, 345202 (2010)
20. National Institute of Standards and Technology [DB]
21. Zhu, X.M., Pu, Y.K.: A simple collisional-radiative model for low-temperature argon discharges with pressure ranging from 1 Pa to atmospheric pressure: kinetics of Paschen 1s and 2p levels. J. Phys. D: Appl. Phys. **43**, 015204 (2010)
22. Li, J., Zhu, X.M., Pu, Y.K.: The population distribution of argon atoms in Paschen 1s levels in an inductively coupled plasma. J. Phys. D: Appl. Phys. **43**, 345202 (2010)
23. Kiehlbauch, M.W., Graves, D.B.: Modeling argon inductively coupled plasmas: the electron energy distribution function and metastable kinetics. J. Appl. Phys. **91**, 3539–3546 (2002)
24. Rauf, S., Kushner, M.J.: Argon metastable densities in radio frequency Ar, Ar/O_2 and Ar/CF4 electrical discharges. J. Appl. Phys. **82**, 2805–2813 (1997)
25. Balamuta, J., Golde, M.F.: Quenching of metastable Ar, Kr, and Xe atoms by oxygen-containing compounds: a resonance fluorescence study of reaction products. J. Chem. Phys. **76**, 2430–2440 (1982)
26. Sadeghi, N., Cheaib, M., Setser, D.W.: Comparison of the Ar($3P_2$) and Ar($3P_0$) reactions with chlorine and fluorine containing molecules: propensity for ion-core conservation. J. Chem. Phys. **90**, 219–231 (1989)
27. Worsley, M.A., Bent, S.F., Fuller, N.C.M., et al.: Characterization of neutral species densities in dual frequency capacitively coupled photoresist ash plasmas by optical emission actinometry. J. Appl. Phys. **100**, 083301 (2006)